Controlling optical bistability via interacting double dark resonances in linear quantum dot molecules

Si-Cong Tian,[1,*] Ren-Gang Wan,[2] Cun-Zhu Tong,[1,3] and Yong-Qiang Ning[1]

[1]*State Key Laboratory of Luminescence and Applications, Changchun Institute of Optics, Fine Mechanics and Physics, Chinese Academy of Sciences, Changchun 130033, China*

[2]*State Key Laboratory of Transient Optics and Photonics, Xi'an Institute of Optics and Precision Mechanics, Chinese Academy of Sciences, Xi'an 710119, China*

[3]*e-mail: tongcz@ciomp.ac.cn*

**Corresponding author: tiansicong@ciomp.ac.cn*

Received June 25, 2014; revised August 20, 2014; accepted September 2, 2014; posted September 5, 2014 (Doc. ID 214469); published October 14, 2014

The behavior of optical bistability (OB) in linear triple quantum dot molecules (QDMs) using double tunneling coupling by means of a unidirectional ring cavity is investigated. The linear and nonlinear susceptibilities of the system are also investigated. The double tunneling between the quantum dots can induce the interaction of double dark resonances, which can enhance the nonlinear response of the system. The type, the hysteresis loop, and the threshold of OB can be controlled by the intensity of the double tunneling and the detuning of the probe field. Our results give insights for future experiments and applications in optics using QDMs. © 2014 Optical Society of America

OCIS codes: (270.0270) Quantum optics; (190.0190) Nonlinear optics; (190.1450) Bistability.
http://dx.doi.org/10.1364/JOSAB.31.002681

1. INTRODUCTION

Optical bistability (OB) has been extensively studied in the recent years because of its potential application in optical logic, all-optical switching, and optical transistors, which are essential for optical computing and communications. OB behavior is the result of nonlinearity of the interactive atomic medium and feedback of the optical interactivity field from the cavity mirrors. Most experimental and theoretical studies in OB are devoted to two-level atomic systems in an optical resonator [1–7]. The OB in three-level atomic systems in optical ring cavity has also been studied theoretically and experimentally [8–14]. One major advantage of using three-level atomic systems instead of two-level atomic systems is that the quantum interference effects induced by optical fields can greatly modify the absorption, dispersion, and nonlinearity of the system [11–13]. In four-level atomic systems, interaction of double dark resonances can be established, which does not occur in three-level systems, allowing modification of the optical response of the atomic medium [15–17]. Therefore, OB in four-level atomic systems via the interaction of double dark resonances has been studied most recently [18].

The above studies are carried out in an atomic medium, and coupling lasers are essential in these systems. On the other hand, two or more quantum dots coupled by tunneling can form quantum dot molecules (QDMs). In QDMs, one can control the tunneling of electrons or holes by an external electric field and create a multilevel structure of excitonic states. Via tunneling coupling, quantum interference and coherence can be produced in QDMs. Using self-assembled dot growth technology, double quantum dots (DQDs) can be fabricated [19]. Many experimental studies have been carried out about such DQDs, such as optical spectroscopy [20], excitonic entanglement [21], single photon and spin storage [22], control of electron tunneling [23], and coherent population trapping [24]. There have also been theoretical works based on DQDs, such as electromagnetically induced transparency (EIT) and slow light [25–27], entanglement [28–31], OB [32–34], coherent population transfer [35], narrowing of the transmission spectrum [36], and narrowing of the fluorescence spectrum [37].

Building on DQDs with controlled electron numbers, both linear and triangular types of triple quantum dots (TQDs) have been achieved [38–41]. In a triangular TQD, we obtained multiple transparency windows and slow light [42]. Later in the same triangular TQD system, Hamedi studied OB with the help of an incoherent pump field [43]. The narrowing transmission spectrum in triangular TQDs has been also investigated [44]. As for a linear TQD, the energy levels and confinement of electrons and holes have been studied experimentally [45,46]. The transmission-dispersion spectrum [47], resonance fluorescence spectrum [48,49], and Kerr nonlinearity [50] have also been investigated theoretically in linear TQDs.

In the present paper, we analyze the controllability of OB via double tunneling in linear TQDs using a unidirectional ring cavity. Our work is based on previous studies of OB, but the scheme proposed here is different from those. First, in contrast with previous studies of OB in atomic systems, in TQDs we use tunneling instead of coupling lasers [8–14,18] to modify OB properties, which can be controlled by the external electric field. Second, although OB properties have been studied in DQDs with one tunneling coupling [32–34], in TQDs the use of double tunneling can induce double dark resonances and provides flexibility in the control of the type, the hysteresis loop, and the threshold of OB. Third, OB has also investigated in quantum wells (QWs) with tunneling coupling

[51,52]. The difference between tunneling coupling QWs and TQDs is that, in QWs, the excited subbands are coupled by tunneling to the same electronic continuum and the laser field couples more than one transition. But in TQDs, the probe field couples only one direct transition, and tunneling couples the other indirect transition. Last, it should be pointed out that OB has recently been studied in another work [43]. Our study is different from that work in the following ways: the system studied here is linear TQDs, while the system of that work is of the triangular type; in our consideration, we do not include the incoherent pump; and we emphasize the double dark resonances and consider both linear and nonlinear susceptibility to explain the physics of OB phenomena.

The paper is organized as follows. In Section 2, we introduce the model and the basic equations of TQDs and the cavity system. In Section 3, we analyze the properties of OB and interpret the corresponding results by linear and nonlinear susceptibilities. Section 4 is the conclusion.

2. MODEL AND EQUATIONS

We consider a TQD sample inside an optical cavity comprising four mirrors, as shown in Fig. 1(a). For simplicity, we assume that mirrors 3 and 4 have 100% reflectivity, and the intensity reflection and transmission coefficient of mirrors 1 and 2 are R and T $(R+T=1)$, respectively. In Fig. 1(b), we show the schematic of the setup of TQDs. Three single QDs are arranged linearly and are coupled together by tunneling. At nanoscale interdot separation, the hole states are localized in the QDs and the electron states are rather delocalized. In TQDs, the tunneling can be controlled by placing a gate electrode between the neighboring dots. Without a gate voltage, the conduction-band electron levels are out of resonance and the electron tunneling between the QDs is very weak, while with a gate voltage, the conduction-band electron levels come close to resonance and the electron tunneling between the QDs is greatly enhanced. The band structure of the TQDs for this situation is shown in Fig. 1(c). (We neglect hole tunneling because of the higher off-resonance of the valence-band energy levels.) Then we give the schematic of the level configuration of TQDs in Fig. 1(d). The ground state $|0\rangle$ has no excitations, while the exciton state $|1\rangle$ has one electron–hole pair in QD 1. Under the tunneling couplings, the electron can tunnel from QD 1 to QD 2, then from QD 2 to QD 3. Therefore, the indirect exciton state $|2\rangle$ has one hole in QD 1 and one electron in QD 2, and indirect exciton state $|3\rangle$ has one hole in QD 1 and one electron in QD 3.

Under the rotating-wave and the electric-dipole approximations, and after performing the unitary transformation $U = e^{-i\omega_p t}(|1\rangle\langle 1| + |2\rangle\langle 2| + |3\rangle\langle 3|)$ [26], which removes the time-dependent oscillatory terms (ω_p is the laser frequency), the Hamiltonian under the basis $\{|0\rangle, |1\rangle, |2\rangle, |3\rangle\}$ can be written as (assumption of $\hbar = 1$)

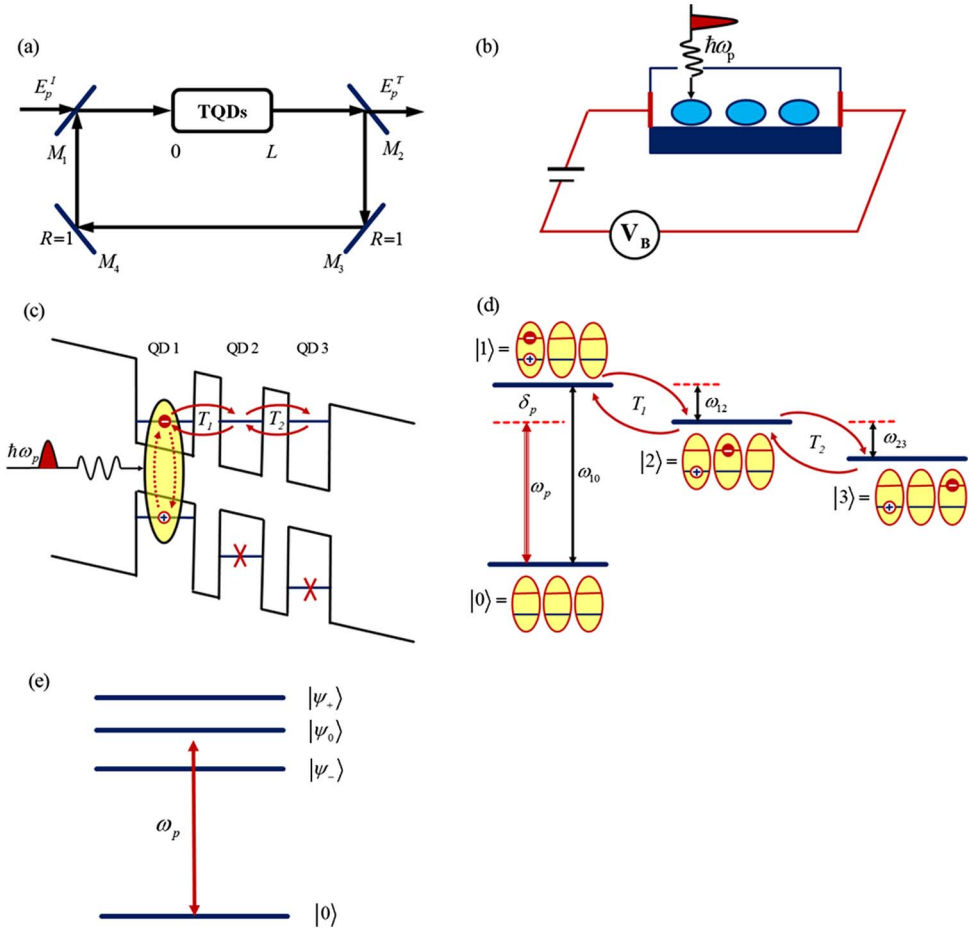

Fig. 1. (a) Unidirectional ring cavity containing a TQD sample of length L. E_p^I and E_p^T are the incident and the transmitted fields, respectively. (b) The schematic of the setup of a TQDs. The probe field transmits QD 1. V_B is a bias voltage. (c) The schematic of the band structure of a TQDs with a gate voltage. (d) The schematic of the level configuration of a TQDs. (e) Dressed states of the TQDs for two tunneling couplings.

$$H_I = \begin{pmatrix} 0 & -\Omega_p & 0 & 0 \\ -\Omega_p & \delta_p & -T_1 & 0 \\ 0 & -T_1 & \delta_p - \delta_1 & -T_2 \\ 0 & 0 & -T_2 & \delta_p - \delta_1 - \delta_2 \end{pmatrix}. \quad (1)$$

Here $\Omega_p = \mu_{10} E_p$ is the Rabi frequency of the transition $|0\rangle \to |1\rangle$. E_p denotes the electric-field amplitude of the laser, and $\mu_{10} = \boldsymbol{\mu}_{10} \cdot \mathbf{e}$ denotes the electric dipole moment for the excitonic transition between states $|0\rangle$ and $|1\rangle$, with $\mathbf{e}$ being the polarization vector. T_1 and T_2 are the tunneling couplings, which depend on the barrier characteristics and the external electric field. $\delta_p = \omega_{10} - \omega_p$, $\delta_1 = \omega_{12}$, and $\delta_2 = \omega_{23}$ are the detuning of the probe field and the tunneling, with ω_{mn} being the transition frequency between $|m\rangle$ and $|n\rangle$ states. Experimentally, the frequency transition ω_{12} and ω_{23} can be done by manipulation of the external electric field that changes the effective confinement potential.

At any time t, the state vector can be written as

$$|\Psi_I(t)\rangle = a_0(t)|0\rangle + a_1(t)|1\rangle + a_2(t)|2\rangle + a_3(t)|3\rangle. \quad (2)$$

The evolution of the state vector obeys the Schrödinger equation

$$\frac{d}{dt}|\Psi_I(t)\rangle = -iH_I(t)|\Psi_I(t)\rangle. \quad (3)$$

By substituting Eq. (1) and Eq. (2) into Eq. (3), and then using the Weisskopf–Wigner theory [53,54], we can obtain the following dynamical equations for atomic probability amplitudes in the interaction picture:

$$i\dot{a}_0 = -\Omega_p a_1, \quad (4a)$$

$$i\dot{a}_1 = -\Omega_p a_0 - T_1 a_2 + (\delta_p - i\gamma_1) a_1, \quad (4b)$$

$$i\dot{a}_2 = -T_1 a_1 - T_2 a_3 + (\delta_p - \delta_1 - i\gamma_2) a_2, \quad (4c)$$

$$i\dot{a}_3 = -T_2 a_2 + (\delta_p - \delta_1 - \delta_2 - i\gamma_3) a_3, \quad (4d)$$

$$|a_0|^2 + |a_1|^2 + |a_2|^2 + |a_3|^2 = 1. \quad (4e)$$

Here, $\gamma_i = \frac{1}{2}\Gamma_{i0} + \gamma_{i0}^d (i = 1-3)$ is the typical effective decay rate, with Γ_{i0} being the radiative decay rate of populations from $|i\rangle \to |0\rangle$ and γ_{i0}^d being the pure dephasing rates.

When the TQDs are inside the optical cavity, because only one probe laser field is applied, the total electromagnetic field is $E = E_p e^{-i\omega_p t} + \text{c.c.}$, where the probe field E_p circulates in the ring cavity, and the symbol "c.c." means complex conjugation. Then, under slowly varying envelope approximation, the dynamic response of the probe field is governed by Maxwell's equation:

$$\frac{\partial E_p}{\partial t} + c\frac{\partial E_p}{\partial z} = i\frac{\omega_p \Gamma}{2\varepsilon_0} P(\omega_p), \quad (5)$$

where c is the speed of light, ε_0 is the permittivity of the free space, and Γ is the optical confinement factor [55]. $P(\omega_p)$ is the slowly oscillating term of the induced polarization in the intersubband transitions $|0\rangle \to |1\rangle$ and is determined by $P(\omega_p) = N\mu_{10}\rho_{10}$. Here, N is the electron density of the TQDs, and $\rho_{10} = a_0 a_1^*$ is the density matrix element, which can be calculated by solving Eq. (4).

We consider the field of Eq. (5) in the steady-state case. By setting the time derivative in Eq. (5) equal to zero for the steady state, we can obtain the field amplitude as follows:

$$\frac{\partial E_p}{\partial z} = i\frac{N\omega_p \mu_{10} \Gamma}{2c\varepsilon_0}\rho_{10}. \quad (6)$$

For a perfectly tuned ring cavity, in the steady-state limit, the boundary conditions impose the following conditions between the incident field E_p^I and the transmitted field E_p^T:

$$E_p(0) = \sqrt{T}E_p^I + RE_p(L), \quad (7a)$$

$$E_p(L) = E_p^T/\sqrt{T}, \quad (7b)$$

where L is the length of the TQD sample, and the second term on the right-hand side of Eq. (7a) describes a feedback mechanism due to the mirror, which is essential to give rise to bistability, that is to say, no bistability can occur if $R = 0$.

In the mean-field limit [56,57], by using the boundary conditions [Eq. (7)] and normalizing the fields by letting $y = \mu_{10}E_p^I/\hbar\sqrt{T}$ and $x = \mu_{10}E_p^T/\hbar\sqrt{T}$, we can get the input–output relationship:

$$y = x - iC\rho_{10}, \quad (8)$$

where $C = LN\omega_p|\mu_{10}|^2\Gamma/2\hbar c\varepsilon_0 T$ is the electronic cooperation parameter. It is worth pointing out that the second term on the right-hand side of Eq. (8) is vital for OB to occur. Then we can arrive at the steady-state solutions of the output field intensity versus the input field intensity.

Because OB behavior is the result of nonlinearity of the interactivity atomic medium and feedback of the optical interactivity field from the cavity mirrors, the investigation of nonlinear susceptibilities of TQDs is necessary. As is known, the probe susceptibility χ is proportional to the density matrix element ρ_{10}. Then, by using the method used in Ref. [50], we obtain the analytical expressions of the first $\chi^{(1)}$ and third $\chi^{(3)}$ order susceptibilities:

$$\chi^{(1)} = \frac{\Gamma|\boldsymbol{\mu}_{10}|^2}{V\varepsilon_0\hbar}\frac{1}{\Gamma_1 - \frac{T_1^2\Gamma_3}{\Gamma_2\Gamma_3 - T_2^2}}, \quad (9a)$$

$$\chi^{(3)} = \frac{\Gamma|\boldsymbol{\mu}_{10}|^4}{3V\varepsilon_0\hbar^3}\frac{1}{\Gamma_1 - \frac{T_1^2\Gamma_3}{\Gamma_2\Gamma_3 - T_2^2}}\frac{1}{\left|\Gamma_1 - \frac{T_1^2\Gamma_3}{\Gamma_2\Gamma_3 - T_2^2}\right|^2} \left(1 + T_1^2\frac{\Gamma_3^2}{|\Gamma_2\Gamma_3 - T_2^2|^2} + (T_1T_2)^2\frac{1}{|\Gamma_2\Gamma_3 - T_2^2|^2}\right), \quad (9b)$$

with $\Gamma_1 = \delta_p - i\gamma_1$, $\Gamma_2 = \delta_p - \delta_1 - i\gamma_2$, and $\Gamma_3 = \delta_p - \delta_1 - \delta_2 - i\gamma_3$; V is the volume of the TQDs [55].

In the following, we present some numerical results for the steady state of the output field intensity versus the input field intensity under various parametric conditions according to Eq. (8) and interpret the results by the linear and nonlinear behavior of TQDs according to Eq. (9).

3. RESULTS AND DISCUSSION

DQDs have been previously fabricated [19,20] and many experimental works based on them have been carried out [21–24]. Building on DQDs, linear TQDs have resulted in much progress [38–40], and the energy levels and confinement of electrons and holes of linear TQDs have been investigated experimentally [45,46]. In such TQDs, the tunneling T_1 and T_2 depend on the barrier characteristics and the external electric field. Frequency transitions ω_{12} and ω_{23} can be done by manipulation of the external electric field, which changes the effective confinement potential. In addition, in this investigation, we work in the low-temperature regime, and consider both the population decay rates and the dephasing rates. Realistic values of the parameters are according to Table 1 of Ref. [50] and references therein. Although some of the parameter values are for DQDs, it can be inferred that the tunneling, energy splitting, and decay rates of TQDs have the same values as those of DQDs. For simplicity, all the parameters are scaled by the decay rate γ_1.

First we show in Fig. 2(a) the OB behavior without the tunneling, with only one tunneling and with double tunneling by the gate voltage. Without the tunneling coupling, the electron cannot tunnel from QD 1 to other QDs. Therefore, the system is reduced to a single QD with one exited state $|1\rangle$ and one ground state $|0\rangle$, and a OB is obtained (red solid line). Then, with only tunneling T_1, the electron can tunnel from QD 1 to QD 2, but cannot tunnel from QD 2 to QD 3. Thus, the system is similar to DQDs, and the OB (black dotted line). With both tunneling T_1 and T_2, the electrons can tunnel from QD 1 to QD 2, and from QD 2 to QD 3, which creates a four-level structure. In this case, the OB appears again (blue dashed line). As can be seen by comparing the blue dashed line and red solid line, the OB threshold y_{th} with double tunneling is smaller than that without double tunneling, while the slope of the lower branches of the two OBs are the same.

The OB behavior can be understood by displaying the linear absorption $\text{Im}[\chi^{(1)}]$, nonlinear absorption $\text{Im}[\chi^{(3)}]$, and nonlinear dispersion $\text{Re}[\chi^{(3)}]$ versus the frequency detuning of the probe field δ_p in Figs. 2(b), 2(c), and 2(d), respectively. When $\delta_p = 0$, it can be seen that the values of linear absorption, nonlinear absorption, and nonlinear dispersion with only one tunneling are all zero (black dotted line), which leads to the disappearance of OB. On the other hand, the value of linear and nonlinear absorption without double tunneling (red solid line) and with double tunneling (blue dashed line) both have nonzero value. Meanwhile, the values of the nonlinear dispersion of these two cases are zero; therefore, the OB obtained in Fig. 2(a) is absorptive. We can also note that the values of linear absorption without double tunneling and that with double tunneling are the same, but the value of nonlinear absorption without double tunneling is smaller than that with double tunneling. Therefore, together with Fig. 2(a), we conclude that first, the linear absorption is relative to the slope of the lower branch of OB. Second, the nonlinear absorption is relative to the absorptive OB threshold: the larger is the value of the nonlinear absorption, the smaller is the OB threshold.

The physical interpretation can be seen clearly under the dressed-state picture. With two tunneling couplings, T_1 and T_2, the state $|1\rangle$ splits into three dressed sublevels [Fig. 1(e)], and the expressions of the three dressed sublevels for $\delta_1 = \delta_2 = 0$ are

$$|\psi_+\rangle = \frac{1}{\sqrt{2}}\left(|1\rangle + |2\rangle + \frac{T_2}{T_1}|3\rangle\right), \tag{10a}$$

$$|\psi_-\rangle = \frac{1}{\sqrt{2}}\left(|1\rangle - |2\rangle + \frac{T_2}{T_1}|3\rangle\right), \tag{10b}$$

$$|\psi_0\rangle = -\frac{T_2}{T_1}|1\rangle + |3\rangle. \tag{10c}$$

From Eq. (10), when $T_2 = 0$, the two dressed levels $|\psi_\pm\rangle$ correspond to the usual Autler–Townes dressed components,

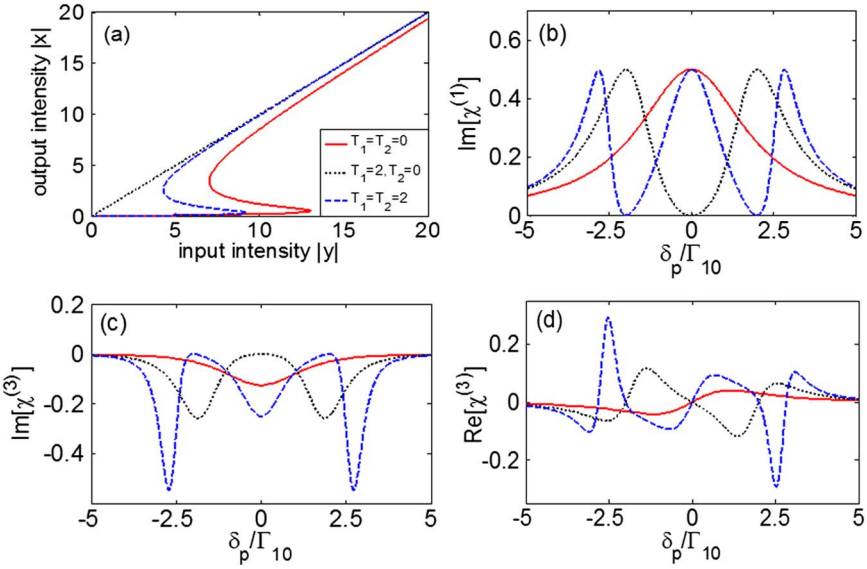

Fig. 2. (a) Output intensity $|x|$ versus input intensity $|y|$, (b) imaginary $\text{Im}[\chi^{(1)}]$ parts of the linear susceptibility, (c) imaginary $\text{Im}[\chi^{(3)}]$, and (d) real $\text{Re}[\chi^{(3)}]$ parts of the nonlinear susceptibility as a function of probe detuning δ_p, respectively. Curves with red solid line, dark dotted line, and blue dashed line correspond to $T_1 = T_2 = 0$, $T_1 = 2, T_2 = 0$, and $T_1 = T_2 = 2$, respectively. Other parameters are $\delta_p = \delta_1 = \delta_2 = 0$, $\gamma_2 = \gamma_3 = 10^{-3}\gamma_1$, and $C = 50$. (All parameters are scaled by the decay rate γ_1.)

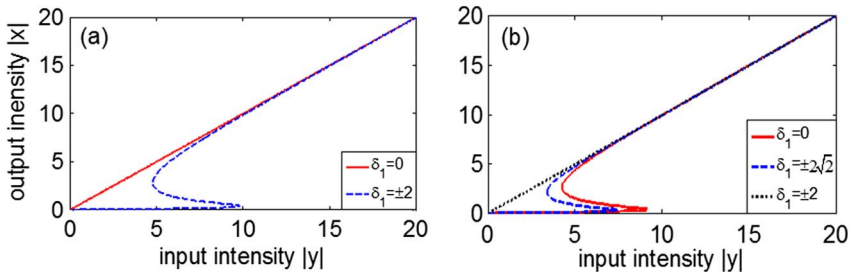

Fig. 3. (a) Output intensity $|x|$ versus input intensity $|y|$ of DQDs ($T_1 = 2, T_2 = 0$). Curves with red solid line and blue dashed line correspond to $\delta_p = 0$ and $\delta_p = \pm 2$, respectively. (b) Output intensity $|x|$ versus input intensity $|y|$ of TQDs ($T_1 = T_2 = 2$). Curves with red solid line, blue dashed line, and dark dotted line correspond to $\delta_p = 0$, $\delta_p = \pm 2\sqrt{2}$, and $\delta_p = \pm 2$, respectively. Other parameters are the same as those in Fig. 2.

and the energy splitting of them is $2T_1$. The other dressed level $|\psi_0\rangle$ coincides with the bare state $|3\rangle$ and, hence, is decoupled from the system. Because both levels $|\psi_\pm\rangle$ have a finite overlap with the excited state $|1\rangle$, there is quantum interference in two probe transitions $|0\rangle \rightarrow |\psi_\pm\rangle$, leading to a single dark resonance. The single dark resonance suppresses the linear and nonlinear absorption when $\delta_p = 0$, resulting in the disappearance of the OB. On the other hand, when $T_2 \neq 0$, the dressed level $|\psi_0\rangle$ contains an admixture of $|1\rangle$ and, thus, has a nonzero dipole matrix element with ground state $|0\rangle$. That is to say, all the dressed levels $|\psi_i\rangle (i = 0, +, -)$ have a finite overlap with the excited state $|1\rangle$. Therefore, there is quantum interference in three probe transitions $|0\rangle \rightarrow |\psi_i\rangle (i = 0, +, -)$, which leads to the double dark resonances. The interaction of the double dark resonances enhances both the linear and nonlinear absorption for $\delta_p = 0$, and, therefore, the OB appears again with smaller OB threshold.

The detuning of the probe field can also influence OB behavior. We plot in Fig. 3 the OB curves in the presence of one tunneling and double tunneling for $\delta_p \neq 0$. When only tunneling T_1 is applied, there are two absorption peaks located at $\delta_p = \pm T_1$, corresponding to the Autler–Townes dressed components. So when $\delta_p = \pm T_1 = \pm 2$, the linear and nonlinear absorption both have maximum value [black dotted lines of Figs. 2(b) and 2(c)]. As a result, the OB appears [blue dashed line of Fig. 3(a)]. Meanwhile, the value of nonlinear dispersion is still zero [black dotted line of Fig. 2(d)]; therefore, the OB is absorptive. The symmetrical linear and nonlinear susceptibility curves make the two OB curves for $\delta_p = 2$ and $\delta_p = -2$ coincident.

As for double tunneling coupling, because of tunneling T_2, one dark resonance splits into two dark resonances, which locate at the position of $\delta_p = \pm T_2$. Therefore, when $\delta_p = \pm T_2 = \pm 2$, the values of linear and nonlinear absorption [blue dashed lines of Figs. 2(b) and 2(c)] are both zero, leading to the disappearance of the OB [black dotted line of Fig. 3(b)]. However, when $\delta_p = \pm\sqrt{T_1^2 + T_2^2} = \pm 2\sqrt{2}$, the linear and nonlinear absorption both have maximum values, and, therefore, the OB appears with two coincident curves [blue dashed line of Fig. 3(b)]. Compared with the case of $\delta_p = 0$, the value of nonlinear absorption is increased [blue dashed line of Fig. 2(c)], while the value of nonlinear dispersion is still zero [blue dashed line of Fig. 2(d)], which leads to the decreased threshold of absorptive OB. On the other hand, the values of linear absorption for $\delta_p = \pm 2\sqrt{2}$ and $\delta_p = 0$ are equal [blue dashed line of Fig. 2(b)], and, therefore, the slopes of the lower branches of OB are the same.

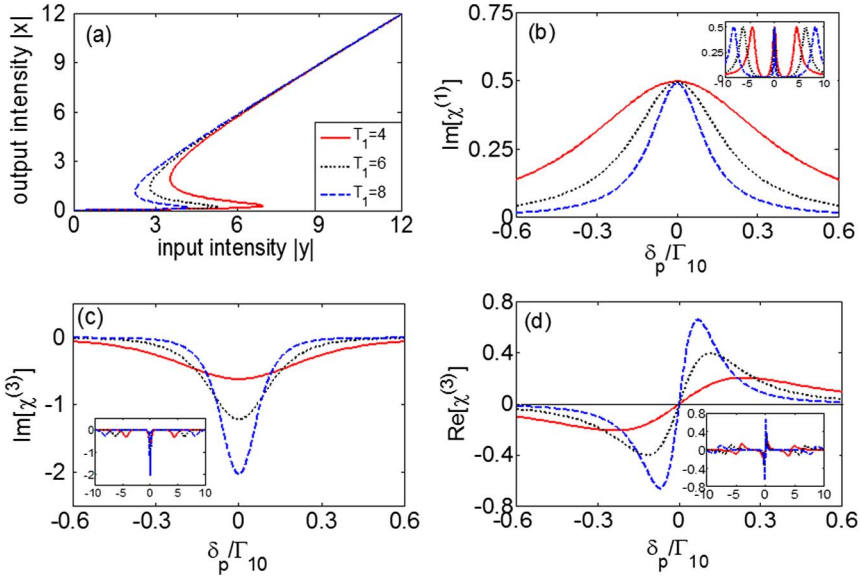

Fig. 4. (a) Output intensity $|x|$ versus input intensity $|y|$, (b) imaginary $\mathrm{Im}[\chi^{(1)}]$ parts of the linear susceptibility, (c) imaginary $\mathrm{Im}[\chi^{(3)}]$, and (d) real $\mathrm{Re}[\chi^{(3)}]$ parts of the nonlinear susceptibility as a function of probe detuning δ_p, respectively. Curves with red solid line, dark dotted line, and blue dashed line correspond to $T_1 = 4$, $T_1 = 6$, and $T_1 = 8$, respectively. The insets are plotted for a larger range of δ_p. Other parameters are the same as those in Fig. 2.

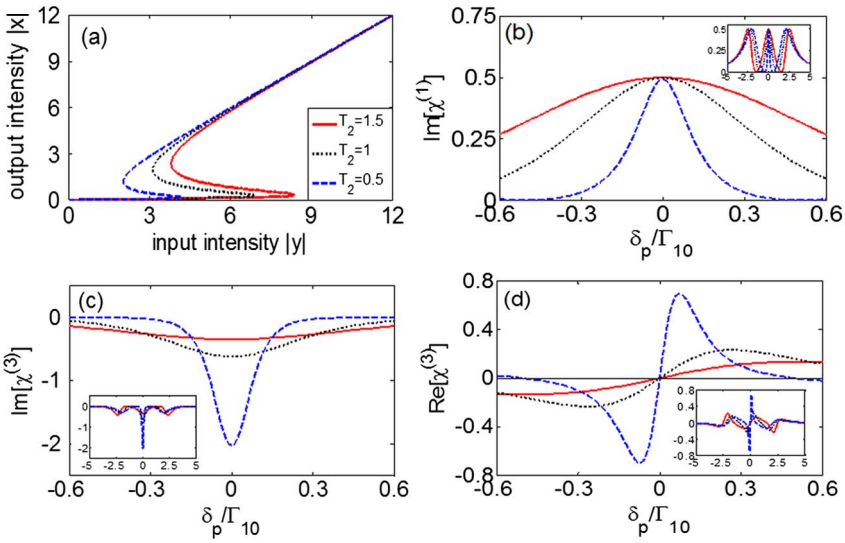

Fig. 5. (a) Output intensity $|x|$ versus input intensity $|y|$, (b) imaginary $\mathrm{Im}[\chi^{(1)}]$ parts of the linear susceptibility, (c) imaginary $\mathrm{Im}[\chi^{(3)}]$, and (d) real $\mathrm{Re}[\chi^{(3)}]$ parts of the nonlinear susceptibility as a function of probe detuning δ_p, respectively. Curves with red solid line, dark dotted line, and blue dashed line correspond to $T_2 = 1.5$, $T_2 = 1$, and $T_2 = 0.5$, respectively. The insets are plotted for a larger range of δ_p. Other parameters are the same as those in Fig. 2.

In Figs. 4 and 5 we show the effects of the intensity of double tunneling coupling on the OB for $\delta_p = 0$. It can be seen from Fig. 4(a) that, for increasing intensity of tunneling T_1, the threshold of OB is decreased, while the slope of the lower branch of OB stays the same. The reason for the results is presented below. As can be seen from Fig. 4(b), in the region of $\delta_p = 0$, the values of linear absorption for different values of T_1 are the same, which leads to the same slope of the lower branch of OB. On the other hand, increasing intensity of tunneling T_1 leads to increased nonlinear absorption [Fig. 4(c)], while the value of nonlinear dispersion stays zero for $\delta_p = 0$ [Fig. 4(d)]. Therefore, for all values of T_1, the OB is absorptive, and the increasing nonlinear absorption results in the decreased threshold of OB.

The changing of the intensity of tunneling T_2 can also lead to the difference of OB. With decreasing value of T_2, the slope of the lower branch of the OB stays the same, while the OB threshold is decreased. The same slope of the lower branch is also due to the same value of linear absorption [Fig. 5(b)], and the decreased threshold of OB is due to the increasing value of nonlinear absorption [Fig. 5(c)]. Because of the zero value of nonlinear dispersion [Fig. 5(d)], the OB is also absorptive.

From the results obtained in Figs. 4 and 5, it can be concluded that the behavior of such absorptive OB can be controlled by the intensity of the tunneling. The increasing intensity of tunneling T_1 or the decreasing intensity of tunneling T_2 can lower the threshold of OB and keep the slope of the lower branch of the OB the same. The physical interpretation is that the increasing intensity of tunneling T_1 or the decreasing intensity of tunneling T_2 can lead to the enhancement of the interaction between the two dark resonances, which results in increased nonlinear absorption, and, therefore, the OB threshold is decreased.

The results of Figs. 4 and 5 are obtained for $\delta_p = 0$. For further investigation, we plot in Fig. 6 the OB of TQDs for $\delta_p = 0.3$ with different intensity of double tunneling. As shown in Fig. 6(a), when the intensity of tunneling T_1 is increasing, the slope of the lower branch of OB is increased and the threshold of OB is decreased. The results can be seen clearly from Figs. 4(b)–4(d). As shown in Fig. 4(b), when $\delta_p = 0.3$, the value of linear absorption is decreased with the increasing value of T_1, and, as a result, the slope of the lower branch of OB is increased. For $T_1 = 4$ or $T_1 = 6$, the values of nonlinear absorption [Fig. 4(c)] and nonlinear dispersion [Fig. 4(d)] are not zero; thus the type of OB is hybrid absorptive–dispersive. Compared between these two cases, the value of nonlinear dispersion is almost the same, while the value of nonlinear absorption of $T_1 = 6$ is smaller than that of $T_1 = 4$, which gives rise to the decreasing threshold of OB. When tunneling T_1 is increased to $T_1 = 8$, the nonlinear

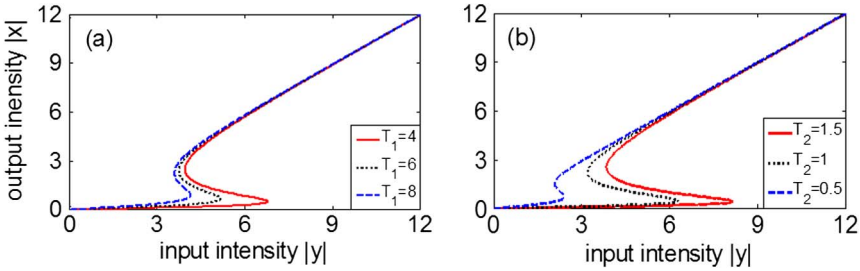

Fig. 6. (a) Output intensity $|x|$ versus input intensity $|y|$ for fixed value of $T_2 = 2$ and different value of T_1. Curves with red solid line, dark dotted line, and blue dashed line correspond to $T_1 = 4$, $T_1 = 6$, and $T_1 = 8$, respectively. (b) Output intensity $|x|$ versus input intensity $|y|$ for a fixed value of $T_1 = 2$ and different values of T_2. Curves with red solid line, dark dotted line, and blue dashed line correspond to $T_2 = 1.5$, $T_2 = 1$, and $T_2 = 0.5$, respectively. Other parameters are the same as those in Fig. 2.

absorption is reduced to zero, so the hybrid absorptive–dispersive OB turns to dispersive OB. Although the value of nonlinear dispersion is smaller than those of $T_1 = 4$ and $T_1 = 6$, the OB threshold is still reduced. Therefore, it can be inferred that the nonlinear dispersion can also influence the threshold of OB.

On the other hand, changing the intensity of tunneling T_2 can also influence OB behavior for $\delta_p = 0.3$. Figure 6(b) shows that the decreasing intensity of tunneling T_2 leads to increased slope of the lower branch of OB and the decreased threshold of OB. The results can be interpreted in Figs. 5(b)–5(d). It can be seen in Fig. 5(b) that with decreasing intensity of tunneling T_2, the value of linear absorption is decreased, which results in increased slope of the lower branch of OB. When $T_2 = 1.5$ and $T_2 = 1$, the values of nonlinear absorption [Fig. 5(c)] are almost the same, but the value of nonlinear dispersion [Fig. 5(d)] of $T_2 = 1$ is larger than that of $T_2 = 1.5$, which leads to the decreased threshold of OB. When $T_2 = 0.5$, the value of nonlinear absorption is reduced to zero, and the value of nonlinear dispersion is smaller than that of the above two cases, so the OB threshold is reduced. This is because, with the decreasing value of tunneling T_2, the hybrid absorptive–dispersive OB turns to the dispersive OB.

4. CONCLUSIONS

In this paper, we explored the intensity of double tunneling coupling and probe detuning on the characteristics of OB in TQDs by means of a unidirectional ring cavity. We found that the type, hysteresis loop, and threshold of OB can be flexibly controlled by these parameters. The double tunneling between the QDs can induce interaction of double dark resonances and enhance the nonlinear response of the system, which is responsible for the behavior of OB. Our scheme may be used for building more efficient optical switches and logic-gate optoelectronic devices for optical computing and quantum information processing.

ACKNOWLEDGMENTS

This work is supported by the National Natural Science Foundation of China (Grant Nos. 11304308 and 61176046), the National Basic Research Program of China (Grant No. 2013CB933300), the International Science Technology Cooperation Program of China (No. 2013DFR00730), the Hundred Talents Program of the Chinese Academy of Sciences, and the Jilin Provincial Natural Science Foundation (Grant No. 20140101203JC).

REFERENCES

1. H. M. Gibbs, S. L. McCall, and T. N. C. Venkatesan, "Differential gain and bistability using a sodium-filled Fabry-Perot interferometer," Phys. Rev. Lett. **36**, 1135–1138 (1976).
2. E. Abraham and S. D. Smith, "Optical bistability and related devices," Rep. Prog. Phys. **45**, 815–885 (1982).
3. A. T. Rosenberger, L. A. Orozco, and H. J. Kimble, "Observation of absorptive bistability with two-level atoms in a ring cavity," Phys. Rev. A **28**, 2569–2572 (1983).
4. L. A. Orozco, H. J. Kimble, A. T. Rosenberger, M. L. Asquini, M. Brambilla, and L. M. Narducci, "Single-mode instability in optical bistability," Phys. Rev. A **39**, 1235–1252 (1989).
5. G. Rempe, R. J. Thompson, R. J. Brecha, W. D. Lee, and H. J. Kimble, "Optical bistability and photon statistics in cavity quantum electrodynamics," Phys. Rev. Lett. **67**, 1727–1730 (1991).
6. A. Lambrecht, E. Giacobino, and J. M. Courty, "Optical nonlinear dynamics with cold atoms in a cavity," Opt. Commun. **115**, 199–206 (1995).
7. T. Ackemann, A. Heuer, Yu. A. Logvin, and W. Lange, "Light-shift-induced level crossing and resonatorless optical bistability in sodium vapor," Phys. Rev. A **56**, 2321–2326 (1997).
8. D. F. Wall and P. Zoller, "A coherent nonlinear mechanism for optical bistability from three level atoms," Opt. Commun. **34**, 260–264 (1980).
9. H. Wang, D. J. Goorskey, and M. Xiao, "Bistability and instability of three-level atoms inside an optical cavity," Phys. Rev. A **65**, 011801(R) (2001).
10. A. Joshi and M. Xiao, "Optical multistability in three-level atoms inside an optical ring cavity," Phys. Rev. Lett. **91**, 143904 (2003).
11. W. Harshawardhan and G. S. Agarwal, "Controlling optical bistability using electromagnetic-field-induced transparency and quantum interferences," Phys. Rev. A **53**, 1812–1817 (1996).
12. A. Joshi, A. Brown, H. Wang, and M. Xiao, "Controlling optical bistability in a three-level atomic system," Phys. Rev. A **67**, 041801(R) (2003).
13. A. Joshi, W. Yang, and M. Xiao, "Effect of quantum interference on optical bistability in the three-level V-type atomic system," Phys. Rev. A **68**, 015806 (2003).
14. J. T. Sheng, U. Khadka, and M. Xiao, "Realization of all-optical multistate switching in an atomic coherent medium," Phys. Rev. Lett. **109**, 223906 (2012).
15. M. D. Lukin, S. F. Yelin, M. Fleishhauer, and M. O. Scally, "Quantum interference effects induced by interacting dark resonances," Phys. Rev. A **60**, 3225–3228 (1999).
16. Y. C. Chen, Y. A. Liao, H. Y. Chiu, J. J. Su, and I. A. Yu, "Observation of the quantum interference phenomenon induced by interacting dark resonances," Phys. Rev. A **64**, 053806 (2001).
17. S. F. Yelin, V. A. Sautenkov, M. M. Kash, G. R. Welch, and M. D. Lukin, "Nonlinear optics via double dark resonances," Phys. Rev. A **68**, 063801 (2003).
18. M. Mahmoudi, S. M. Mousavi, and M. Sahrai, "Controlling the optical bistability via interacting dark-state resonances," Eur. Phys. J. D **57**, 241–246 (2010).
19. L. Wang, A. Rastelli, S. Kiravittaya, M. Benyoucef, and O. G. Schmidt, "Self-assembled quantum dot molecules," Adv. Mater. **21**, 2601–2618 (2009).
20. E. A. Stinaff, M. Scheibner, A. S. Bracker, I. V. Ponomarev, V. L. Korenev, M. E. Ware, M. F. Doty, T. L. Reinecke, and D. Gammon, "Optical signatures of coupled quantum dots," Science **311**, 636–639 (2006).
21. D. Kim, S. G. Carter, A. Greilich, A. S. Bracker, and D. Gammon, "Ultrafast optical control of entanglement between two quantum-dot spins," Nat. Phys. **7**, 223–229 (2011).
22. A. Boyer de la Giroday, N. Sköld, R. M. Stevenson, I. Farrer, D. A. Ritchie, and A. J. Shields, "Exciton-spin memory with a semiconductor quantum dot molecule," Phys. Rev. Lett. **106**, 216802 (2011).
23. K. Müller, A. Bechtold, C. Ruppert, M. Zecherle, G. Reithmaier, M. Bichler, H. J. Krenner, G. Abstreiter, A. W. Holleitner, J. M. Villas-Boas, M. Betz, and J. J. Finley, "Electrical control of interdot electron tunneling in a double InGaAs quantum-dot nanostructure," Phys. Rev. Lett. **108**, 197402 (2012).
24. K. M. Weiss, J. M. Elzerman, Y. L. Delley, J. Miguel-Sanchez, and A. Imamoğlu, "Coherent two-electron spin qubits in an optically active pair of coupled InGaAs quantum dots," Phys. Rev. Lett. **109**, 107401 (2012).
25. C. H. Yuan and K. D. Zhu, "Voltage-controlled slow light in asymmetry double quantum dots," Appl. Phys. Lett. **89**, 052115 (2006).
26. H. S. Borges, L. Sanz, J. M. Villas-Bôas, O. O. Diniz Neto, and A. M. Alcalde, "Tunneling induced transparency and slow light in quantum dot molecules," Phys. Rev. B **85**, 115425 (2012).
27. S. Michael, W. W. Chow, and H. C. Schneider, "Group-velocity slowdown in a double quantum dot molecule," Phys. Rev. B **88**, 125305 (2013).
28. X. Y. Lü, J. Wu, L. L. Zheng, and Z. M. Zhan, "Voltage-controlled entanglement and quantum-information transfer between spatially separated quantum-dot molecules," Phys. Rev. A **83**, 042302 (2011).

29. M. T. Cheng, X. S. Ma, Y. Q. Luo, P. Z. Wang, and G. X. Zhao, "Entanglement generation and quantum state transfer between two quantum dot molecules mediated by quantum bus of plasmonic circuits," Appl. Phys. Lett. **99**, 223509 (2011).
30. A. S. Zheng, Y. J. Cheng, and J. B. Liu, "Voltage-controlled multipartite entanglement with distant quantum dot molecules via adiabatic-varying tunnel coupling," J. Opt. Soc. Am. B **30**, 3168–3173 (2013).
31. S. P. Liu, R. Yu, J. H. Li, and Y. Wu, "Generation of a multi-qubit W entangled state through spatially separated semiconductor quantum-dot-molecules in cavity-quantum electrodynamics arrays," J. Appl. Phys. **115**, 134312 (2014).
32. J. Li, R. Yu, J. Liu, P. Huang, and X. Yang, "Voltage-controlled optical bistability of a tunable three-level system in a quantum-dot molecule," Physica E **41**, 70–73 (2008).
33. Z. P. Wang, S. L. Zhen, X. Q. Wu, J. Zhu, Z. G. Cao, and B. L. Yu, "Controllable optical bistability via tunneling induced transparency in quantum dot molecules," Opt. Commun. **304**, 7–10 (2013).
34. H. Jafarzadeh, M. Sahrai, and K. Jamshidi-Ghaleh, "Controlling the optical bistability in a three-level quantum-dot molecule via gate voltage and indirect incoherent pump field," Eur. Phys. J. D **68**, 115 (2014).
35. E. Voutsinas, A. F. Terzis, and E. Paspalakis, "Control of indirect exciton population in an asymmetric quantum dot molecule," Phys. Lett. A **378**, 219–225 (2014).
36. Y. D. Peng, Y. P. Niu, N. Cui, and S. Q. Gong, "Cavity linewidth narrowing by voltage-controlled induced transparency in asymmetry quantum dot molecules," Opt. Commun. **284**, 824–827 (2011).
37. S. C. Tian, C. Z. Tong, C. L. Wang, L. J. Wang, H. Wu, E. B. Xing, Y. Q. Ning, and L. J. Wang, "Spectral line narrowing via spontaneously generated coherence in quantum dot molecules," Opt. Commun. **312**, 296–301 (2014).
38. C. Y. Hsieh, Y. P. Shim, M. Korkusinski, and P. Hawrylak, "Physics of lateral triple quantum-dot molecules with controlled electron numbers," Rep. Prog. Phys. **75**, 114501 (2012).
39. Q. H. Xie, A. Madhukar, P. Chen, and N. P. Kobayashi, "Vertically self-organized InAs quantum box islands on GaAs(100)," Phys. Rev. Lett. **75**, 2542–2545 (1995).
40. G. Rainò, A. Salhi, V. Tasco, M. De Vittorio, A. Passaseo, R. Cingolani, M. De Giorgi, E. Luna, and A. Trampert, "Structural and optical properties of vertically stacked triple InAs dot-in-well structure," J. Appl. Phys. **103**, 096107 (2008).
41. R. Songmuang, S. Kiravittaya, and O. G. Schmidt, "Formation of lateral quantum dot molecules around self-assembled nanoholes," Appl. Phys. Lett. **82**, 2892–2894 (2003).
42. S. C. Tian, C. Z. Tong, R. G. Wan, Y. Q. Ning, and L. J. Wang, "Tunneling induced transparency and controllable group velocity in triple and multiple quantum-dot molecules," arXiv:1310.4599 (2013).
43. H. R. Hamedi, "Inter-dot tunneling control of optical bistability in triple quantum dot molecules," Physica B **449**, 5–9 (2014).
44. S. C. Tian, R. G. Wan, E. B. Xing, C. Z. Tong, and Y. Q. Ning, "Tunneling control of cavity linewidth narrowing via quantum interference in triangular quantum dot molecules," J. Mod. Opt. **61**, 1479–1485 (2014).
45. M. Hayne and R. Provoost, "Electron and hole confinement in stacked self-assembled InP quantum dots," Phys. Rev. B **62**, 10324–10328 (2000).
46. V. Popescu, G. Bester, M. C. Hanna, A. G. Norman, and A. Zunger, "Theoretical and experimental examination of the intermediate-band concept for strain-balanced (In,Ga)As/Ga(As,P) quantum dot solar cells," Phys. Rev. B **78**, 205321 (2008).
47. R. Yu, J. H. Li, C. L. Ding, and X. X. Yang, "Transmission-dispersion characteristics of waveguide-coupled photonic crystal two-mode nanocavity embedding three tunnel-coupled quantum dots," Phys. Lett. A **375**, 2738–2746 (2011).
48. S. C. Tian, C. Z. Tong, C. L. Wang, and Y. Q. Ning, "Effects of spontaneously generated coherence on resonance fluorescence from triple quantum dot molecules," J. Lumin. **153**, 169–176 (2014).
49. S. C. Tian, R. G. Gang, C. Z. Tong, Y. Q. Ning, L. Qin, and Y. Liu, "Tunneling induced dark states and the controllable resonance fluorescence spectrum in quantum dot molecules," J. Phys. B **47**, 155503 (2014).
50. S. C. Tian, R. G. Gang, C. Z. Tong, Y. Q. Ning, L. Qin, and Y. Liu, "Giant Kerr nonlinearity induced by tunneling in triple quantum dot molecules," J. Opt. Soc. Am. B **31**, 1436–1442 (2014).
51. J. H. Li, "Controllable optical bistability in a four-subband semiconductor quantum well system," Phys. Rev. B **75**, 155329 (2007).
52. J. H. Li, X. Y. Hao, J. B. Liu, and X. X. Yang, "Optical bistability in a triple semiconductor quantum well structure with tunnelling-induced interference," Phys. Lett. A **372**, 716–720 (2008).
53. G. S. Agarwal, *Quantum Optics* (Springer-Verlag, 1974).
54. S. M. Barnett and P. M. Radmore, *Methods in Theoretical Quantum Optics* (Oxford University, 1997).
55. J. Kim, S. L. Chuang, P. C. Ku, and C. J. Chang-Hasnain, "Slow light using semiconductor quantum dots," J. Phys. Condens. Matter **16**, S3727–S3735 (2004).
56. R. Bonifacio and L. A. Lugiato, "Optical bistability and cooperative effects in resonance fluorescence," Phys. Rev. A **18**, 1129–1144 (1978).
57. P. Meystre, "On the use of the mean-field theory in optical bistability," Opt. Commun. **26**, 277–280 (1978).